Flow-Structural Interaction in Solid Rocket Motors

John W. Murdock and William A. Johnston
Distinguished Engineer and Senior Project Engineer
The Aerospace Corporation
P. O. Box 92957 – M4-964
Los Angeles, CA 90009-2957
USA

SUMMARY

This article reviews and summarizes recent work on flow-structural interaction in solid motors. This interaction is important because it can lead to rocket motor failure. In the first part of the document, an idealized model of the failure mechanism is developed to illustrate in simple terms how such an event can occur. In the second part of this article recently published numerical modeling work, which models flow-structural interactions in some detail, is summarized. The static test failure of the Titan solid rocket motor upgrade (SRMU) that occurred on 1 April 1991 demonstrated the importance of flow-structural modeling in the design of large solid rocket motors.

INTRODUCTION

The first discussion, known to us, of the possibility that an interaction between the propellant grain and the motor flow field could cause motor failure is in Wimpress (1950). He shows various curves with a critical value of the elastic modulus, E, below which, "there is no finite equilibrium pressure…and the motor blows up."

Bartley and Mills (1959) also discuss grain instability in tubular, internal solid motors. Their model also shows that for the grain geometry considered, there is a critical propellant modulus, below which the motor fails.

Glick, Cavney, and Thurman (1967) modeled a bore constriction failure of the Castor II motor that occurred at a propellant slot. They point out that the stability of the propellant can be significantly enhanced if the propellant downstream of the slot has a radius. They state that H. W. Ritchey first suggested the use of such a radius and they term it a Ritchey radius.

There was a flurry of activity in the area of flow-structural interaction subsequent to the Titan SRMU test failure. The initial efforts were aimed at understanding the failure and analyzing the new Titan design to make sure the problem was fixed (Johnston and Murdock [1995], Chang, Patel, and Yang [1994], Cosstephens [1995], Johnson and Lauterbach [1992]). This work was followed by analyses of other existing or new motors, to make sure that they were designed with an adequate safety margin (Johnston [1996], Wang, Yang, Than, and Ndefo [1994]). This work is reviewed in some detail in the latter part of this document.

An important goal of this article is to assure that the possibility of flow-structural interaction leading to a motor failure is not forgotten or overlooked – as it seems to have been in the period between 1967 and 1991.

Paper presented at the RTO/VKI Special Course on "Internal Aerodynamics in Solid Rocket Propulsion", held in Rhode-Saint-Genèse, Belgium, 27-31 May 2002, and published in RTO-EN-023.

Report Documentation Page

Form Approved
OMB No. 0704-0188

1. REPORT DATE	2. REPORT TYPE	3. DATES COVERED
00 JAN 2004	**N/A**	**-**

4. TITLE AND SUBTITLE	5a. CONTRACT NUMBER
Flow-Structural Interaction in Solid Rocket Motors	5b. GRANT NUMBER
	5c. PROGRAM ELEMENT NUMBER
6. AUTHOR(S)	5d. PROJECT NUMBER
	5e. TASK NUMBER
	5f. WORK UNIT NUMBER
7. PERFORMING ORGANIZATION NAME(S) AND ADDRESS(ES) **The Aerospace Corporation P. O. Box 92957 M4-964 Los Angeles, CA 90009-2957 USA**	8. PERFORMING ORGANIZATION REPORT NUMBER
9. SPONSORING/MONITORING AGENCY NAME(S) AND ADDRESS(ES)	10. SPONSOR/MONITOR'S ACRONYM(S)
	11. SPONSOR/MONITOR'S REPORT NUMBER(S)

12. DISTRIBUTION/AVAILABILITY STATEMENT
Approved for public release, distribution unlimited

13. SUPPLEMENTARY NOTES
See also ADM001656., The original document contains color images.

14. ABSTRACT

15. SUBJECT TERMS

16. SECURITY CLASSIFICATION OF:			17. LIMITATION OF ABSTRACT	18. NUMBER OF PAGES	19a. NAME OF RESPONSIBLE PERSON
a. REPORT	b. ABSTRACT	c. THIS PAGE			
unclassified	**unclassified**	**unclassified**	**UU**	**18**	

Standard Form 298 (Rev. 8-98)
Prescribed by ANSI Std Z39-18

A SIMPLE PHYSICAL MODEL OF GRAIN INSTABILITY

We are interested in the interaction of the propellant grain and the motor flow that can produce a catastrophic motor failure. How can such a thing occur? Examination of known failures shows that they have been initiated by events occurring either at transverse slots in the grain or at the location of joints of multi-segment motors.

The flow past one such slot is shown in Fig. 1. The flow impinges on the upstream-facing propellant and raises the pressure on that face. The flow also expands around the corner of the grain and reduces the pressure on the interior of the bore. The combination of these two forces causes the flow area to constrict, as shown in Fig. 1. If the elastic modulus of the propellant grain is too low or the local bore flow rate is too high, then unconstrained deflection of the grain can occur. This will fracture the propellant grain and/or block the motor bore. Either of these events will be catastrophic for the motor.

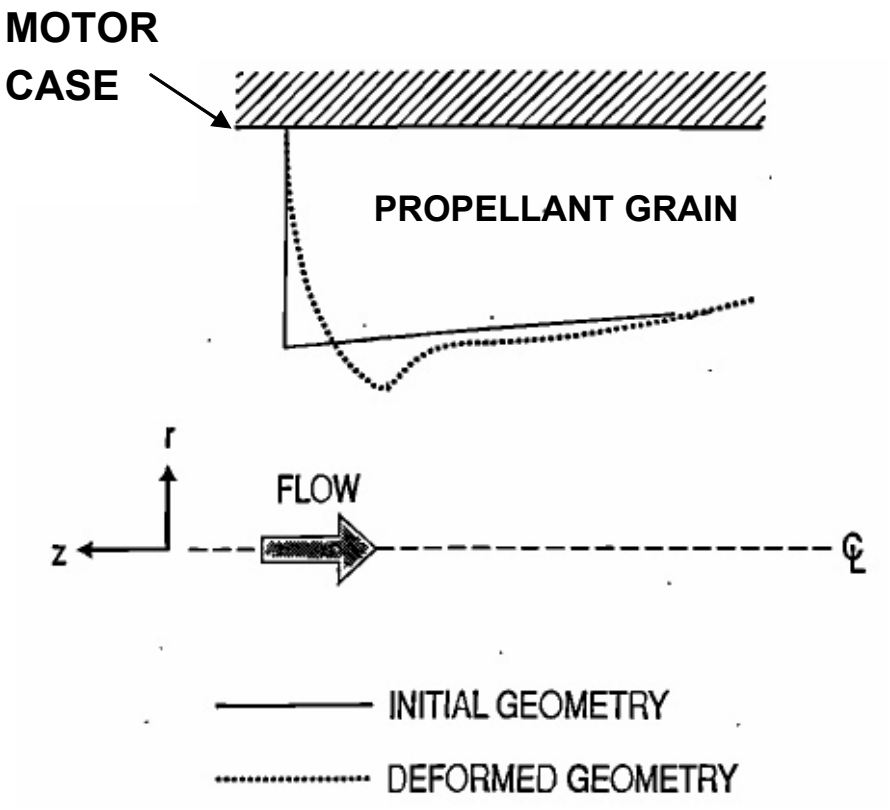

Figure 1: Schematic of Failure Mechanism.

In order to give a simple physical picture of the flow-structural instability that can lead to grain and motor failure, a very simple, analytical model is constructed to illustrate how such a failure occurs. With this in mind, the emphasis will be on simplicity rather than fidelity with the real physical situation.

In accord with this approach, we model the flow through the constriction in Fig. 1 as a choked, perfect gas flow. This gives the simple expression

$$W = KPA \tag{1}$$

where W is the mass flow rate past the bore constriction, P is the stagnation pressure upstream of the constriction, A is the area of the bore constriction, and K is a constant that is easily obtained from gas-dynamic theory. [See, for example, Shapiro (1953).] We note here that a well-designed motor bore would never have locally sonic flow, so that eq. (1) is an approximation. The main justification for its use is the simplicity; eq. (1) could be replaced with the orifice equation for subsonic-flow, but the subsequent analytical solutions would have to be replaced with less obvious numerical solutions. Also, observe that if a bore-constriction failure does occur, the flow is likely to choke during that process.

It is convenient to use a dimensionless version of eq. (1) and normalize the mass flow rate and pressure with their nominal values that would be obtained with an undeformed grain area A_0.

$$w = \frac{W}{W_0} \tag{2}$$

$$p = \frac{P}{P_0} \tag{3}$$

$$a = \frac{A}{A_0} \tag{4}$$

With this normalization, eq. (1) becomes

$$w = pa \tag{5}$$

and the constant in eq. (1) is related to the normalization constants by

$$K = \frac{W_0}{P_0 A_0} \tag{6}$$

The second half of the model relates the bore area to the pressure. In keeping with maximum simplicity, a linear relation between the area and pressure is used. (Letting the bore radius decrease linearly with pressure results in a somewhat more complicated mathematical model with some improvements to the physical model. Predictions made with both models are compared with Titan SRMU data in the following section.)

$$A = A_0 - CP \tag{7}$$

In eq. (7), C is a constant of proportionality that varies as the reciprocal of the elastic modulus of the propellant.

Putting eq. (7) in dimensionless form, gives the result

$$a = 1 - \left(\frac{CP_0}{A_0} \right) p = 1 - cp \tag{8}$$

where the dimensionless version of the constant C is implicitly defined by eq. (8).

Equations (5) and (8) can be combined and either the pressure or the bore area eliminated. Elimination of the area, results in a quadratic equation with solutions

$$p = \frac{1 \pm \sqrt{1 - 4cw}}{2c} \tag{9}$$

Equation (9) has real solutions only for

$$w \le \frac{1}{4c} \tag{10}$$

The solutions to eq. (9) are plotted in Fig. 2 as a function of the reciprocal stiffness parameter of the propellant, c. The dimensionless mass flow rate produced by the propellant has been taken to be constant, with a value of unity; this approximation implies that the propellant grain is a flow source. The flow from the propellant grain is actually a weak function of pressure – so this is a reasonable approximation.

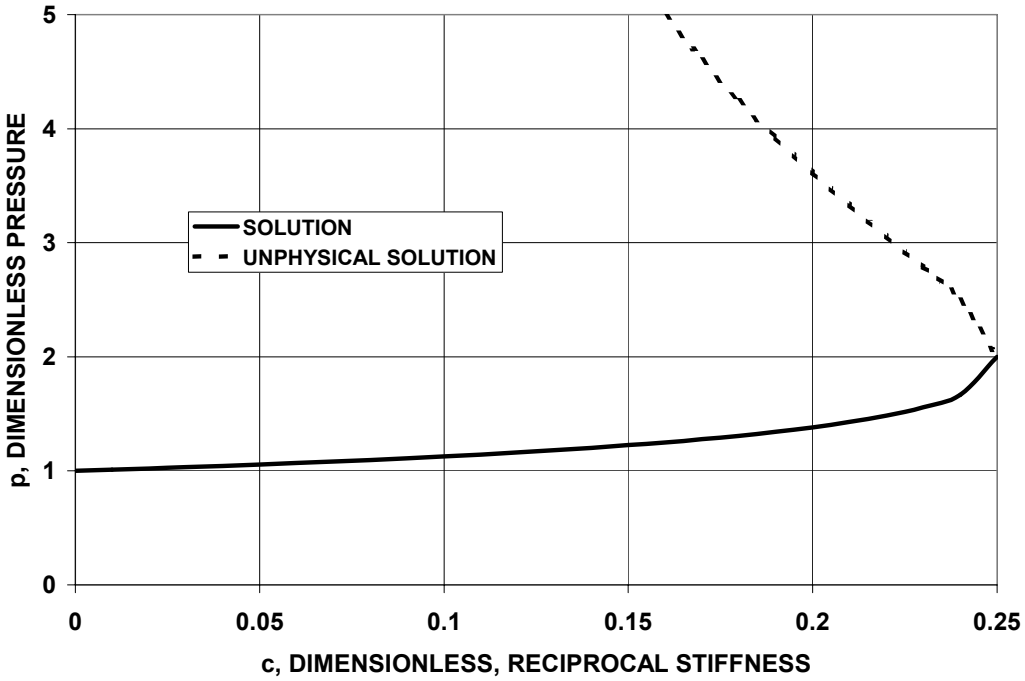

Figure 2: Model Problem with $w = 1$.

The two solutions to eq. (9) are shown in Fig. 2. The lower locus of solutions has positive slope and can occur physically; the solutions on the upper curve are physically unrealizable. (If one were somehow able to start out on the upper curve, the flow state would immediately jump to the other, lower-energy curve.) The two solutions are connected at the point at which the product of w and c is a maximum (or in the case of Fig. 2, maximum c). This critical value occurs when the equality in eq. (10) is satisfied. The models of Wimpress (1950) and Bartley and Mills (1959) also show double-valued solution curves, only one of which is physically realizable. As both these articles point out, attempts to operate beyond the critical point will cause the motor to blow up.

In summary, the very simple model developed here shows that at low flow rates or high propellant modulus, there are two solutions to the model equations. Only one of these solutions has physical significance. These two solutions join and terminate at a critical flow rate given in dimensionless terms by the equality in eq. (10) and in dimensional terms by

$$W_{crit} = \frac{KA_0^2}{4C} \tag{11}$$

The motor has no operating point for flows exceeding the critical one defined by eq. (11). This model illustrates how the grain and the flow can couple and result in an unstable motor. Furthermore, the physics of this simple model is the same as in the large-scale numerical models used previously to study this phenomenon and discussed subsequently.

APPLICATION OF SIMPLE MODEL TO TITAN SRMU

It is interesting to apply the simple model developed in the previous section to the Titan failure to assess its validity, since the critical flow rate only depends on three parameters.

The first parameter in eq. (11) is simply the constant relating pressure, flow rate, and area for choked flow. This constant can easily be obtained from the known motor pressure, motor flow rate, and nozzle flow area. Table 1 gives the relevant Titan SRMU constants and the value of K computed from the values in the first three lines of the table.

Table 1: Selected Titan SRMU Parameters

Motor mass flow rate, Mg/s	W^*	18.8
Motor chamber pressure, MPa	P_c	7.45
Nozzle throat area, m^2	A^*	0.535
Choked flow constant, ms/m	K	4.72
Specific heat ratio	γ	1.13
Sonic pressure ratio	P^*/P_c	0.578
Mass flow from forward two segments, Mg/s	W_{12}	13.2
Propellant elastic modulus (at failure), MPa	E	8.2

The other two parameters can be obtained from Fig. 3, which is obtained from Johnston and Murdock (1995). (This paper will be discussed in more detail, subsequently. For now we are only concerned with Fig. 3.)

$$\begin{bmatrix} \Delta r_A \\ \Delta z_A \\ \Delta r_B \end{bmatrix} = \frac{1}{E} \cdot \begin{pmatrix} 685.538 & -194.376 & 52.573 & -686.516 & 231.231 \\ 805.881 & -110.236 & 193.040 & -849.259 & 403.428 \\ 69.042 & -0.272 & 28.567 & -28.362 & 4.402 \end{pmatrix} \cdot \begin{bmatrix} P_1 \\ P_2 \\ P_3 \\ P_4 \\ P_5 \end{bmatrix}$$

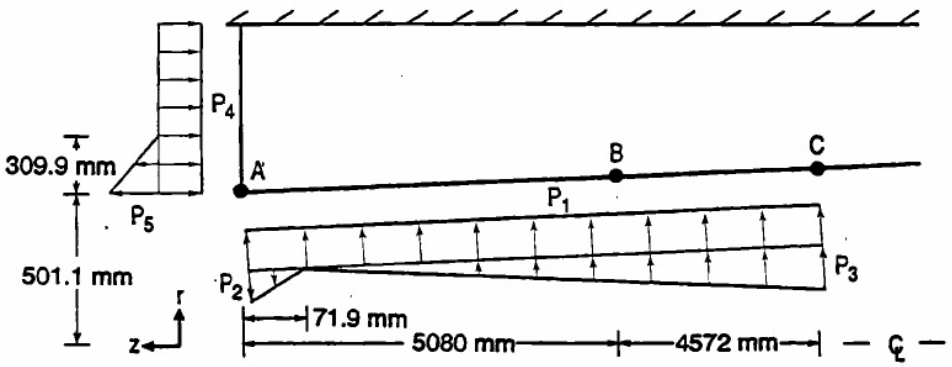

Figure 3: Structural Influence Coefficients for the Aft Propellant Segment, Titan SRMU.

The figure shows the initial diameter of the grain at point A. This is the forward corner of the aft propellant segment and is the known location of the grain collapse. The radius of 501 mm gives a value of A_0 of 0.789 m^2.

The matrix operator in Fig. 3 also shows the structural influence coefficients of the aft propellant section. These coefficients were obtained from a series of grain structural analyses carried out using the ABAQUS (1989) code. The grain deformations can be obtained by multiplying the coefficient matrix by the indicated pressure loads. The quantity E is the propellant modulus (MPa); P_1, P_2, P_3, P_4, and P_5 are the values of the depicted pressure loads (MPa); Δr_A, Δz_A, and Δr_B are the radial and axial displacements (mm) of points A, B, which are at the corner and midpoint of the segment.

The first row of the matrix in Fig. 3 can be used to compute the rate of change in bore radius with pressure. This can be related to the constant C in the simple model by differentiating eq. (7)

$$C = -\frac{dA}{dP} = -2\pi r \frac{dr}{dP} \tag{12}$$

It is now necessary to relate the single, stagnation pressure in the model to the five pressure loads in Fig. 3. Only the pressures acting at the point A are of interest, so P_3 which does not act at that location is neglected. Two distributed pressure forces act on the left-hand face in Fig. 3, P_4 and P_5. The algebraic sum of these ($P_4 - P_5$ according to the sign convention of Fig. 3) is equated to the variable P used in the present model.

We arbitrarily partition half the pressure to each component. These assumptions give

$$P_4 = P/2 \tag{13}$$

$$P_5 = -P/2 \tag{14}$$

It assumed that the radial pressure acting on point A is the sonic throat pressure, which according to Table 1 is 0.578 times the stagnation pressure. In a similar manner we assume that the algebraic sum of P_1 and P_2 equals the sonic pressure and the partitioning is again equal. This gives

$$P_1 = 0.578P/2 \tag{15}$$

$$P_2 = -0.578P/2 \tag{16}$$

The matrix equation in Fig. 3 can now be used to determine dr/dP, using the approximate propellant modulus at failure, taken from Johnston and Murdock (1995) and replicated in Table 1. Combining this value with eqs. (12) and (11) gives

$$W_{crit} = 9.33\,\text{Mg/s} \tag{17}$$

Comparing this with the flow from the two forward segments, given in Table 1, we see that the simple prediction indicates that a 30 percent lower motor flow than the actual one would have caused a grain with this modulus to collapse. (The model and the present discussion neglect the weak variation of motor flow rate with pressure.)

$$\frac{W_{crit}}{W_{12}} = 0.71 \tag{18}$$

An alternative interpretation is that at the motor flow rate, even if the modulus had been 30 percent higher, the motor would still have failed. Stated still another way, the simple model is conservative by 30 percent compared to the large-scale numerical model.

It was briefly mentioned previously that the simple model could be improved by replacing the linear pressure-area relation, eq. (7), with a linear pressure-radius model. Such a model may be written as

$$R = R_0 - C_R P \tag{19}$$

Combining this equation, rather than eq. (7), with eq. (1) gives a cubic rather than a quadratic equation. Analytical solutions are still possible, but the algebra is more complicated. Skipping the details, an equation for the critical mass flow rate, similar to eq. (11) can be obtained in this case. It is

$$W_{crit} = \frac{4\pi K R_0^3}{27 C_R} \tag{20}$$

Substitution of numerical values into eq. (20), gives

$$W_{crit} = 11.1\,\text{Mg/s} \tag{17}$$

This value is 16 percent lower than the flow from the two forward segments. Thus, this model is conservative by about half as much as the linear pressure-area model.

To summarize, a quite simple model of the grain collapse has been developed to illustrate the physics of this interaction. This model has been applied to the Titan SRMU failure and found to produce reasonable and conservative predictions of the failure. However, we have used in this model the numerically generated influence coefficients for the grain displacement. Thus, the actual application of the model used a combination of fluid mechanical approximations and numerical stress analysis. Even so, this model is significantly simpler than the coupled, unsteady flow-structural interaction calculations discussed subsequently in this document.

It is surprising that this model works as well as it does. As noted, it was developed primarily for illustrative purposes, rather than predictive purposes. Also it has only been compared against a single data point. Any application of this model to new designs should keep these limitations in mind.

COMPLETE MOTOR MODEL

During the ignition transient period of solid rocket motor (SRM) operation, several complex, time-dependent coupled processes occur. In a large segmented SRM, the hot gas from the igniter travels down the bore and heats the propellant surface to ignition; once ignition occurs, the propellant surface becomes a site of gas generation. Since the convective and radiative heat transfer that lead to propellant ignition are dependent on the developing flowfield, and since the development of the internal flowfield is dependent on the rate at which the flame spreads down the motor, the time-dependent flow and surface temperature are coupled. Furthermore, the surface pressure load on the propellant grain causes deformation, which in turn alters the flowfield. This results in additional coupling of the internal flowfield with the propellant geometry. This flow-structural coupling is particularly important in segmented SRMs, in which the propellant segments have forward corners (see Fig. 1) that jut out into the bore at intersegment slots (e.g., Titan 7 segment SRM, Space Shuttle SRM, Titan SRMU, Ariane 5 MPS). When axial flow impinges on a protruding corner, the surface pressure deforms the corner out into the bore and further constricts the flow, which then raises the upstream pressure and exacerbates the pressure loading on the corner. If this feedback loop proves to be unstable, then the corner will continue to deform and the motor to pressurize, until either the grain and/or the motor case fails.

Johnston and Murdock (1995) developed the first, multidimensional, coupled numerical procedure for analysis of the flow-structural interaction. Their computer code simultaneously modeled the developing flowfield and the associated propellant grain deformation during the ignition transient period of SRM operation. It is during this initial period of motor operation, when the propellant surface has receded only a little through burning and erosion, that the pressure differential across propellant segment corners typically is at a maximum and the bore radius at a minimum. It is at this time that the interaction between the grain and the flowfield, and the associated danger of grain and motor case failure, is greatest. The following elements were coupled together to create a code, designed to provide a model of the time-dependent, fluid-solid interaction inside an SRM:

1) An ignition transient flow code (Johnston [1991]), which provides a detailed picture of the time-dependent flowfield and flame spreading inside the motor. The ignition transient flow code is itself created by coupling together an unsteady internal- flow code (Ton, Wang, and Widhopf [1990]) with an unsteady heat conduction solution for the propellant surface temperature.
2) A set of structural influence coefficients, that allows the major features of the grain deformation that result from a given surface pressure distribution to be calculated (Patel and Yang [1991]).

3) A grid-generation code, which generates a grid mesh for the internal-flow passages, based on the deformed shape of the propellant grain. This grid mesh then is used in the ignition transient flow code.

These three elements are needed for any flow-structural interaction code. Further details of these three elements as assembled by Johnston and Murdock (1995) are given in the remainder of this section.

Ignition Transient Flow Solution

Johnston (1991) developed the numerical calculation procedure for treating the ignition transient flowfield. The ignition transient flow solution is a composite calculation. It combines an unsteady, axisymmetric solution of the equations of inviscid fluid motion with semi-empirical models for the convective and radiative heat transfer to the propellant surface during the run-up to ignition. The inviscid, single-phase, single-component flow solution is obtained from a time-marching, finite-volume numerical solution of the Euler equations. This numerical solution, which is spatially second-order accurate and employs the total variation diminishing (TVD) methodology of Harten (1983), is described by Wang and Widhopf (1989) and has been implemented for segmented SRMs by Ton, Wang, and Widhopf (1990). An unsteady, one-dimensional, heat conduction solution for the propellant grain is coupled to this flow solution in order to calculate the propellant surface temperature. Together with a surface temperature ignition criterion, this determines the ignition delay and flame-spreading rate.

Grain Shape Calculation

In the Johnston and Murdock (1995) approach, the grain deformation component in the flow-structural interactive calculation procedure is employed periodically at constant intervals throughout the time-marching process. An interval of 100 time steps between geometry updates was found by experience to provide sufficient time accuracy and to be economically feasible. Since the typical flow solution time step was limited by numerical stability to the order of 10^{-5} s, it follows that the grain shape was recalculated about every millisecond.

The grain deformation calculation itself consists of multiplying (for each propellant segment under consideration) a pressure loads vector by a structural influence coefficient matrix to get the resultant displacements at a few key points, which define the shape of the grain. This procedure was illustrated for the aft segment of the SRMU in Fig. 3 and the details of its implementation were discussed in a previous section.

Note that although the coefficient matrices used therein were relatively small, there is no fundamental limitation on size.

Grid Geometry

The final element needed in the flow-structural interaction calculation is a grid generation package. Many excellent grid generation codes are available today, so that most of the approximations made in some of the earlier work would not be necessary today.

One exception is the treatment of star grains, which are treated with an axisymmetric model to avoid a full three-dimensional computer code. The propellant in the forward closure of the Titan SRMU has a star-grain cross-section with axial grooves. To account for this three-dimensional feature in the axisymmetric model, the axial grooves were omitted, resulting in an annular propellant cross section. The inner radius of this annulus was set so that the void volume in the actual forward segment and the computational forward segment

were matched. Then the burning rate in the forward closure was adjusted upward to account for the discrepancy in the burning area.

Another consideration is the procedure for mapping the numerical solution for the old grid onto the new grid geometry. Johnston and Murdock (1995) used a grid generation code in which the number of flowfield cells did not change nor did the relative position within the mesh change as that mesh undergoes distortion. As a consequence, when a geometry update was carried out, the shape and position of the cells changed only slightly. For this reason, the cell values of pressure, density, temperature, and velocity during the geometry update process were simply carried over.

Although the prior approach gave satisfactory results, a more rigorous approach is to derive the moving boundary finite difference equations for the flow model, as has been done by Wang (1992), and use these equations when the grid is updated. Wang, Yang, Than, and Ndefo (1994) used this approach when they did flow structural calculation for the Titan 7-segment rocket motor. However, one drawback to this more rigorous approach is the requirement to deform the grid and remesh each time step.

LARGE MOTOR SOLUTIONS

There were two consequences of the failure of the Titan SRMU. The first was an extensive effort to model and understand the failure, so that a recurrence could be prevented. Subsequent to this, other large motors were analyzed to make sure there was no chance of a grain failure. Some of these analyses were done before the motors were flown, as in the case of the Ariane V, and some were carried out for motors already flying successfully, such as the Titan 7-segment SRM. The results of these efforts are summarized here.

Titan SRMU Solutions

Johnston and Murdock (1995) carried out several numerical stimulations using the time-dependent, flow-structural interactive procedure described herein in order to simulate the static firing of the Titan SRMU, which occurred on April 1, 1991, at Edwards Air Force Base, California. At about 1.6 s into this static test, the motor case failed due to excessive internal pressure. Chamber pressure measurements obtained just prior to the failure showed the head-end chamber pressure increasing rapidly and the aft-end pressure dropping. This divergence of the head-end and aft-end chamber pressures implies a bore constriction, and strain gauge measurements from various axial locations placed this critical constriction at the aft slot. The probable cause of this bore constriction was judged to be the uncontrolled deformation, or collapse, of the forward corner of the aft propellant segment under the applied pressure load.

Due to the uncertainty in the value of the propellant modulus, and the crucial role that this property plays in the success or failure of the motor, numerical static firing simulations were performed for a range of propellant moduli. Simulations were produced with the modulus represented as a decreasing function of time and with constant modulus. The first type of behavior was intended to model change in effective modulus as the propellant undergoes pressurization. The assumed modulus functions for the four cases considered here are shown in Fig. 4. Also shown in Fig. 4 are the cases in which a grain collapse was or was not predicted.

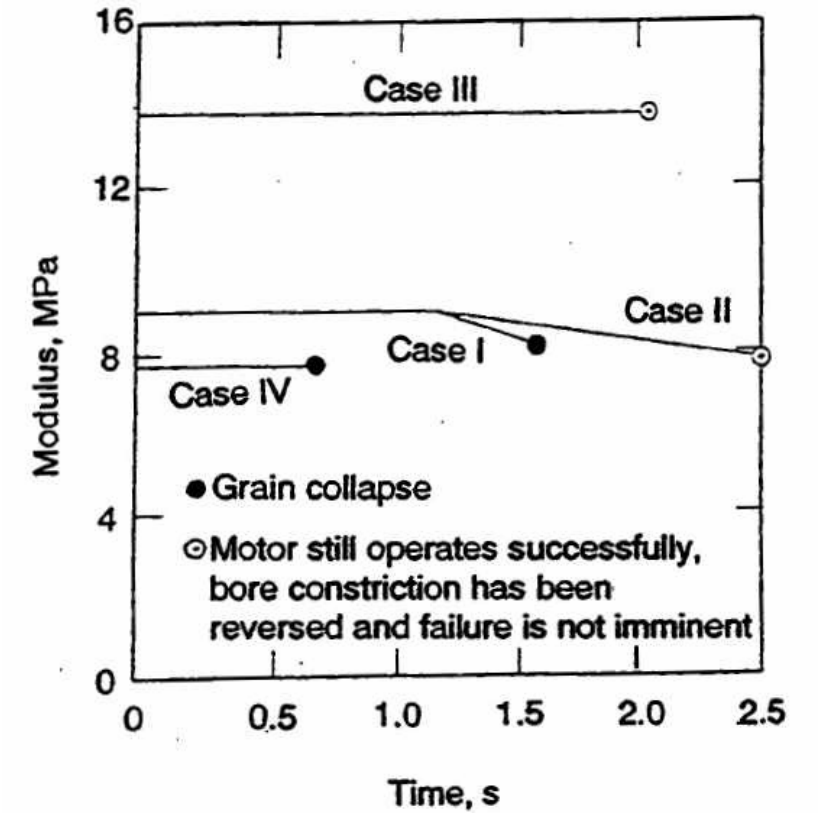

Figure 4: Modulus Functions for Titan SRMU Simulations.

The numerical solution using the modulus shown in Fig. 4 as Case I gave best agreement with the static firing data and is the only result shown herein. The modulus in this case is defined by

$$E = 9.0\,;\ t \le 1.1$$

$$E = 9.0 - 1.7(t - 1.1)\,;\ t > 1.1 \qquad (18)$$

where E is in MPa and t in seconds.

The predictions for Case I are shown in Figs. 5 and 6. The computed bore radii at the forward and aft corners of the center and aft propellant segments are given in Fig. 5. Figure 5 shows that the forward corner of the aft segment is deflected slowly inward for about the first 1.5 s. It then very suddenly collapses to essentially zero, when the motor fails. A comparison of the pressure data at the fore and aft ends of the motor with predictions for the same locations is shown in Fig. 6. The agreement is quite good, except that the run up to failure is slower in the actual case than in the prediction. This disagreement is most probably associated with the approximations made in modeling the propellant modulus by eq. (18).

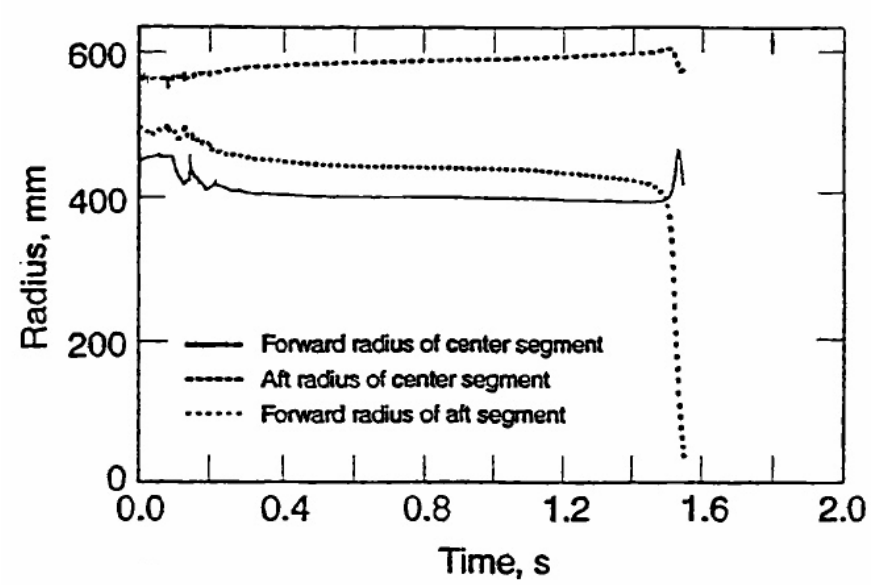

Figure 5: Computed Bore Radii (Case I), Titan SRMU.

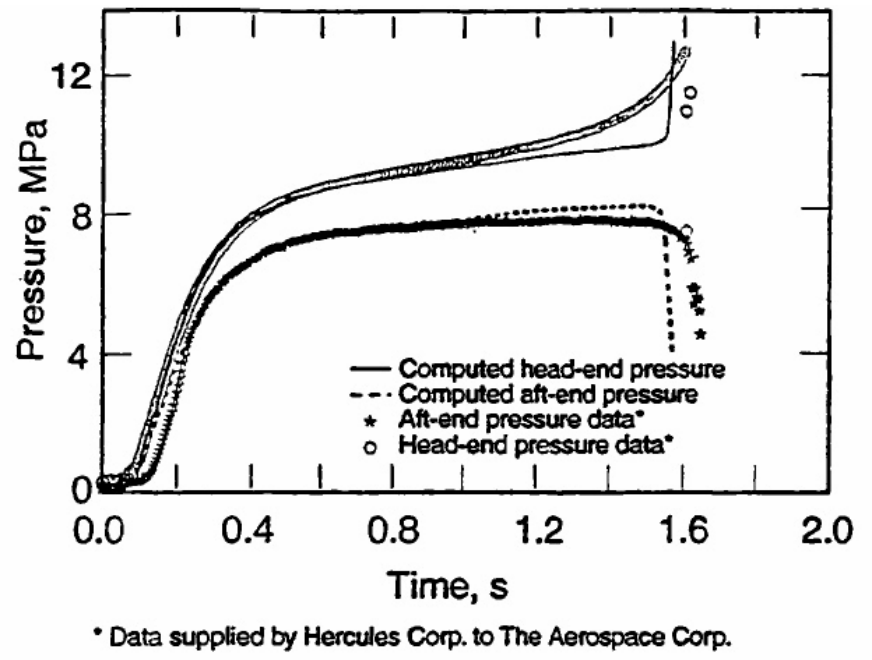

Figure 6: Comparison of Computed (Case I) and Measured Head- and Aft-End Pressures, Titan SRMU.

Since a catastrophic bore constriction arises when forward corners of propellant segments jut out into the bore flow, designs that remove or mitigate this feature will produce a better motor design. The obvious way to do this is to chamfer (i.e., either chop off or round) the forward corners of the segments as shown in Fig. 7.

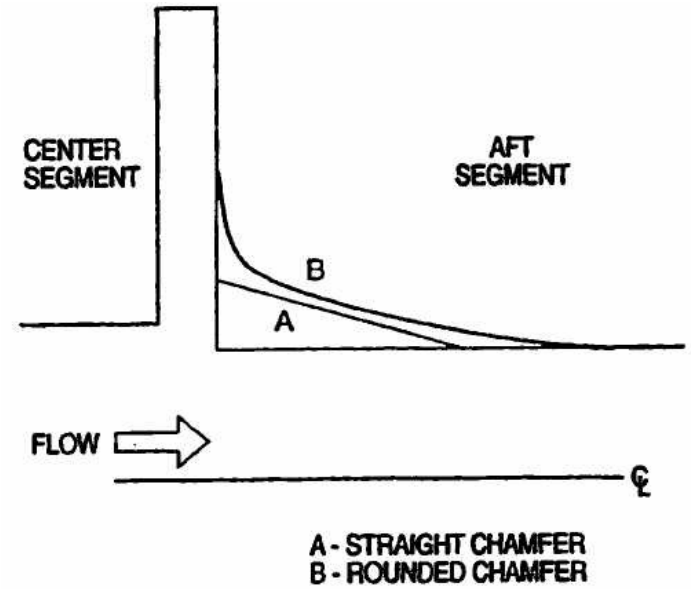

Figure 7: Chamfering Concepts.

Johnston and Murdock (1995) carried out a flow-structural simulation for an SRMU with a straight chamfer at the forward corner of the aft segment, but with the center segment unchanged. This chamfer, which removes a triangular cross-sectional piece from the corner, is shown as A in Fig. 7. The modulus was lowered until the motor failed; the results from this numerical solution may be found in Figs. 8 and 9. This failure was interesting, because in this case the catastrophic bore constriction occurred at the forward corner of the center segment (see Fig. 8). The grain deformation of the aft segment was diminished considerably by the chamfer, and the numerical results indicated that a failure originating at the aft segment would not be possible for this motor.

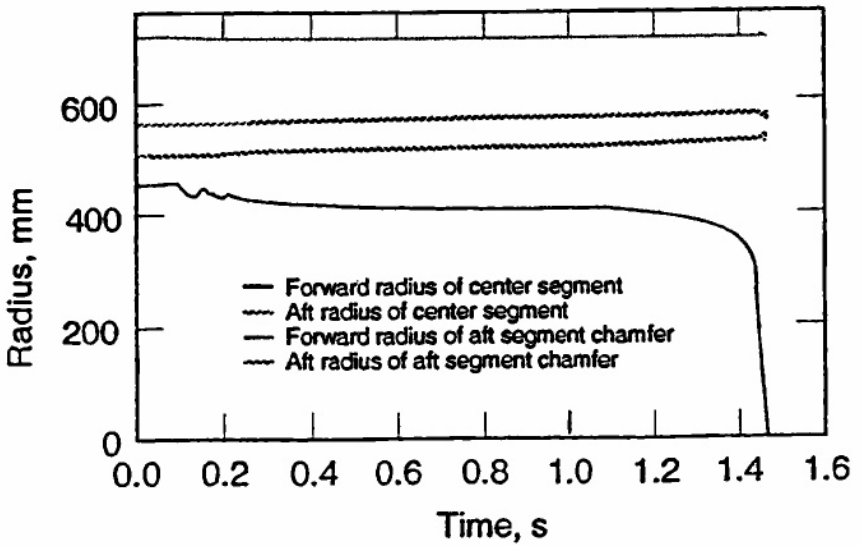

Figure 8: Computed Bore Radii, Titan SRMU, Straight Chamfer on Aft Segment.

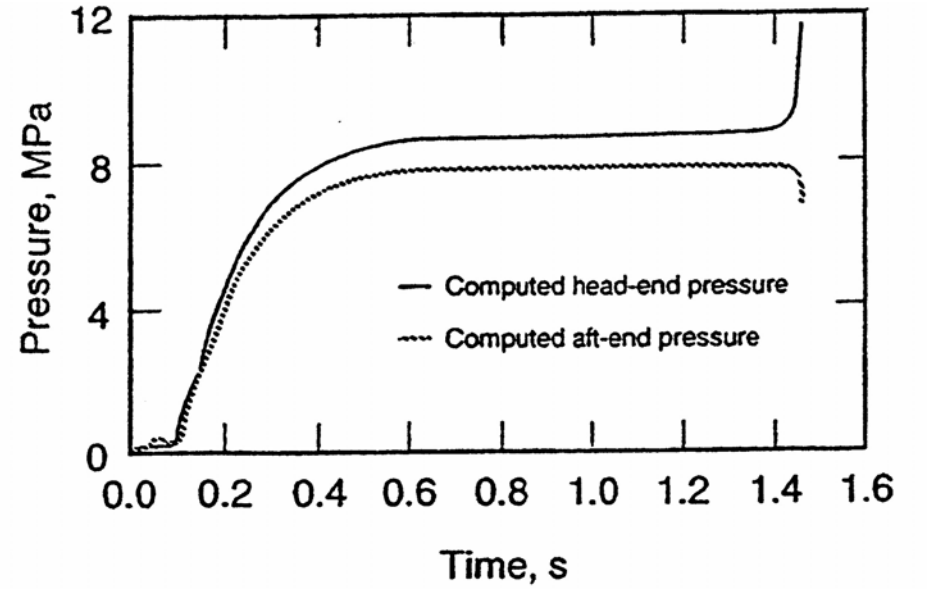

Figure 9: Computed Head- and Aft-End Pressures, Titan SRMU, Straight Chamfer on Aft Segment.

The model developed in the first section of this article shows that, because the flow rate is larger there, the preferred failure site for a motor is the forward corner of the aft-most segment. However, the numerical simulations for the Titan SRMU shown in Figs. 8 and 9 show the forward corner of the center segment can also experience failure. These results suggest that a successful design may require chamfering most or all of the segments in a multi-segment motor.

Ariane 5 MPS Solutions

Johnston (1996) analyzed the Ariane 5 MPS. Despite the fact that this motor has chamfered leading edges of both the center and aft segments, it is susceptible to a grain collapse if the modulus is small enough. (The internal grain geometry and finite difference mesh used to analyze the flow are shown in Fig. 10.)

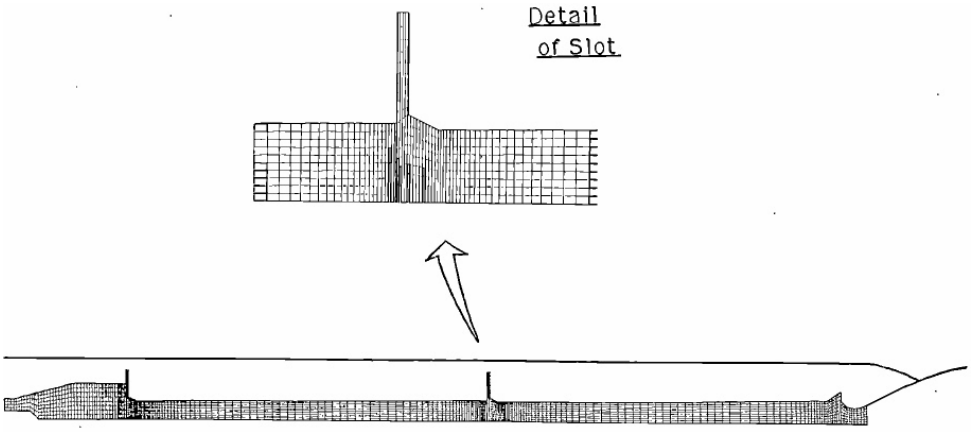

Figure 10: Initial Geometry and Cell Mesh for the Ariane 5 Internal Flowfield.

Johnston found that if the modulus exceeded 500 psi (3.4 MPa) then the grain is stable. However, when he analyzed the case with a propellant modulus of 400 psi (2.8 MPa) he found a grain collapse. These results are shown in Figs. 11 and 12. Figure 11 shows the bore radii and the two corners of the chamfered grain, with the collapse occurring after 0.3 s. The grain oscillations at about 0.1 s are deemed to be non-physical and associated with the fact that the propellant mass and damping are neglected. Since these oscillations damp out before the collapse they are not a concern.

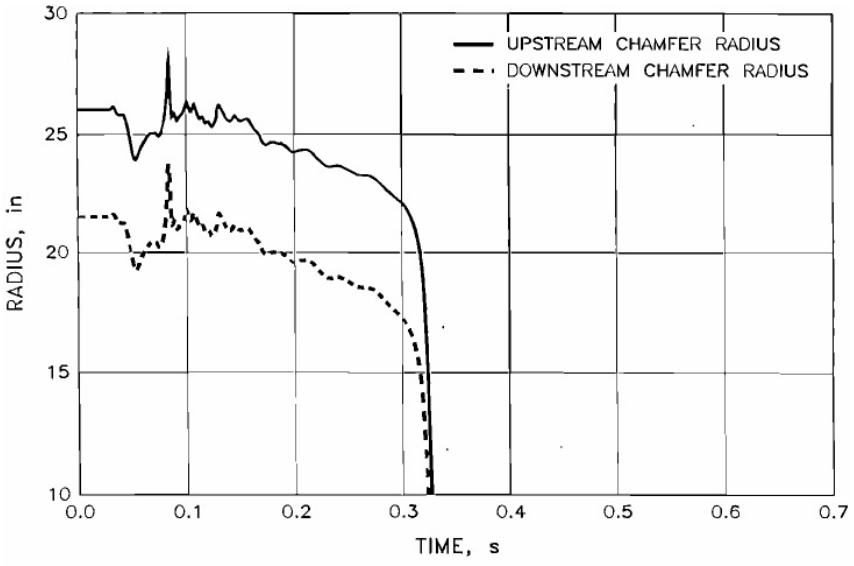

Figure 11: Computed Bore Radii at the Upstream and Downsteam Corners of the Aft Segment Chamfer, Ariane 5 MPS (E = 2.8 MPa).

The divergence of the head- and aft-end pressures at the time of the collapse is shown in Fig. 12.

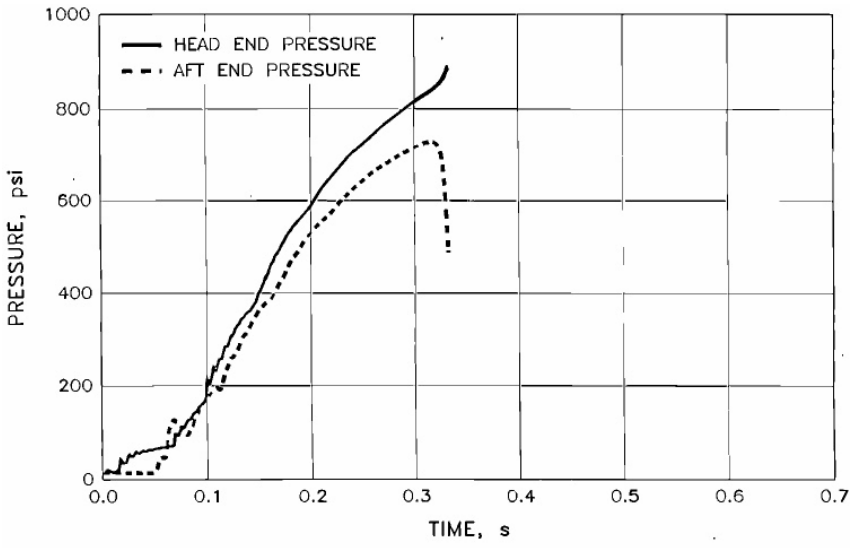

Figure 12: Computed Head- and Aft-End Pressures, Ariane 5 MPS (E = 2.8 MPa).

Titan 7-Segment Solutions

Wang, Yang, Than, and Ndefo (1994) carried out a flow-structural analysis for the Titan IV 7-segment motor. As noted previously, these calculations make fewer grid generation approximations than the earlier models but may expend more computer time. It is again found that if the modulus of the propellant is low enough, a grain collapse will occur. For this motor, the authors found that the Titan 7-segment motor will fail at the corner of the 7th segment if the modulus is 600 psi (4.1 MPa) or less. As expected the failure occurs at the forward end of the last segment, where the flow rate is largest.

CONCLUDING REMARKS

Flow-structural interaction of the bore flow and the propellant grain has caused occasional rocket motor failures. The most notable and recent one is the Titan SRMU. With modern computer methods, this failure mechanism can be modeled and steps, such as chamfering, taken to eliminate it if it is found to be possible.

Even though motor failures of this class had occurred prior to the first test of the Titan SRMU and their cause documented, the possibility of a grain collapse on this motor was overlooked. A possible cause of this oversight is that this failure involves two disciplines, fluid and structural mechanics. Hopefully, this article can help to prevent such a lapse in the future.

REFERENCES

ABAQUS, 1989, *Version 4.8, User's Manual,* Hibbit, Karlson, and Sorensen, Inc., Palo Alto, CA.

Bartley, C.E., and Mills, M.M., 1959, "Solid Propellant Rockets," *Jet Propulsion Engines, Vol. XII, High Speed Aerodynamics and Jet Propulsion,* Ed. O.E. Lancaster, pp. 541-544, Princeton University Press, Princeton.

Chang, I-S., Patel, N.R., and Yang, S., 1994, "Titan IV SRMU Anomaly and Redesign Analyses," AIAA Paper 94-3284.

Cosstephens, S.D., "An Efficient Model for Coupling Solid Rocket Internal Flows with Grain Deformation," AIAA Paper 95-2875.

Glick, R.L., Cavney, L.H., and Thurman, J.L., 1967, "Internal Ballistics of Slotted-Tube, Solid-Propellant Rocket Motors," *Journal of Spacecraft and Rockets*, Vol. 4, No. 4, pp. 525-530.

Harten. A., 1983, "High Resolution Schemes for Hyperbolic Conservation Laws," *Journal of Computational Physics*, Vol. 49, No. 3, pp. 357-393.

Johnson, D.H., and Lauterbach, D.D., 1992, "Coupled Flow-Structural Analysis of the Redesigned Titan IV SRMU," AIAA Paper 92-3825.

Johnston, W.A., 1991, "A Numerical Procedure for the Analysis of the Internal Flow in a Solid Rocket Motor During the Ignition Transient Period," AIAA Paper 91-1655.

Johnston, W.A., 1996, "Flow-Structural Analysis of the Ariane 5 Solid Rocket Motor During Ignition Transient," AIAA Paper 96-0653.

Johnston, W.A., and Murdock, J.W., 1995, "Flow-Structural Interaction Inside a Solid Rocket Motor during Ignition Transient," *Journal of Propulsion and Power*, Vol. 11, No. 5, pp. 998-1005.

Patel, N.R., and Yang, S.H., 1991, Personal Communication, The Aerospace Corp., Los Angeles, CA.

Shapiro, A.H., (1953), *The Dynamics and Thermodynamics of Compressible Fluid Flow,* p. 85, Ronald Press, New York.

Ton, V.T., Wang, J.C.T., and Widhopf, G.F., 1990, "Segmented Solid Rocket Motor Internal Flow Simulations," AIAA Paper 90-0683.

Wang, J.C.T., 1992, "A Full Conservation Finite Volume TVD Algorithm for Initial-Boundary Value Problems with Moving Boundary," *Advances in Computer Methods for Partial Differential Equations – VII,* Ed. V. Vichnevetsky, D. Knight, and G. Richter, pp. 782-787, IMACS, New Brunswick, NJ.

Wang, J.C.T., Yang, S.H., Than, P.T., and Ndefo, E.D., 1994, "Coupled Transient Flowfield and Propellant Deformation Analyses for the Titan IV 7-Segment Solid Rocket Motor," AIAA Paper 94-3285.

Wang, J.C.T., and Widhopf, G.F., 1989, "A High-Resolution TVD Finite Volume Scheme for the Euler Equations in Conservation Form," *Journal of Computational Physics*, Vol. 84, No. 1, pp. 145-173.

Wimpress, R.N., 1950, *Internal Ballistics of Solid-Fuel Rockets,* p. 79, McGraw-Hill, New York.